

iGait: Vision-based Low-Cost, Reliable Machine Learning Framework for Gait
Abnormality Detection

by

SAIF IFTEKAR SAYED

Presented to the Faculty of the Graduate School of
The University of Texas at Arlington in Partial Fulfillment
of the Requirements
for the Degree of

MASTER OF SCIENCE

THE UNIVERSITY OF TEXAS AT ARLINGTON

December 2017

Copyright © by Saif Iftakar Sayed 2017

All Rights Reserved

TABLE OF CONTENTS

LIST OF ILLUSTRATIONS	iv
LIST OF TABLES	vi
Chapter	Page
1. Abstract	1
2. Literature Review	2
2.1 Impact of health on gait	2
2.2 Data Acquisition Types	3
2.3 Chronic Low back pain	8
3. Methodology	10
3.1 The iGait System	10
3.1.1 Body Features Extraction	15
3.1.2 Fall Prediction	22
3.1.3 The iGait System Protocol	24
4. Experimental Results	28
4.1 Experimental Results	28
4.1.1 Classification metrics	28
4.1.2 Feature Significance	31
4.1.3 ROC Curves	35
5. Conclusion and Future Work	39
5.1 Conclusion and Future Work	39
REFERENCES	40

LIST OF ILLUSTRATIONS

Figure	Page
2.1 setup of 3 force resistive resistors(left) and a gyroscope(right)	4
2.2 setup of a BSN sensor behind the ear and a RGB-D Camera	6
2.3 Computation of features at $\mu = 0$ with non-overlapping(a), overlapping(b) and at a viewpoint at $\mu = 20$ (c)	7
2.4 Individual ellipse model attached to the respective segments of the body . . .	8
3.1 Block Diagram of iGait System	11
3.2 Kinect V1 Sensor	12
3.3 Kinect V2 Skeleton Map	13
3.4 Kinect V2 Joints X,Y,Z co-ordinates in meters (green) with the filtered val- ues(red)	14
3.5 Computed Center of Mass X,Y,Z co-ordinates for Normal and Limping walk over number of frames	15
3.6 Hunch angles for normal and limping walks	16
3.7 Anterior angle over a set of consecutive frames and the least square fitted curve.	17
3.8 Mediolateral angle over a set of consecutive frames and the least square fitted curve.	17
3.9 Knee angles for Left and Right leg for Limping and Normal walk.	18
3.10 Elbow angles for Left and Right arms for Limping and Normal walk.	19
3.11 Gradient of difference of left and right ankle position and the corresponding binarized curve	20
3.12 Knee angle difference and fitted curve	20

3.13	x component of left and right hip vs time for lowback pain patients	21
3.14	x component of left and right hip vs time for normal patients	21
3.15	Difference between left and right ankle	22
3.16	Flow diagram of Complete Algorithm	23
3.17	Experimental Setup	24
4.1	MATLAB GUI for recording and classification	29
4.2	Right leg joints highlighted in blue	29
4.3	Feature importance for in-lab experiment	34
4.4	Feature importance for Low-back pain experiment	35
4.5	ROC for Class Index 0	36
4.6	ROC for Class Index 1	36
4.7	ROC for Class Index 2	37
4.8	ROC for Class Index 3	37
4.9	ROC for low back pain Class	38

LIST OF TABLES

Table	Page
3.1 Count of video sequences for experiment	25
4.1 Classification metrics for in-lab experiments	30
4.2 Classification metrics for Low-back pain patients	31
4.3 List of features used in the experiments and their respective indices used in Fig. 4.3 and 4.4.	32
4.4 List of features used in the experiments and their respective indices used in Fig. 4.3 and 4.4(Continued).	33
4.5 Metrics (top 5 features) for in-lab experiments	34
4.6 Metrics (top 5 features) for low-back pain experiments	34

CHAPTER 1

Abstract

Human gait has shown to be a strong indicator of health issues under a wide variety of conditions. For that reason, gait analysis has become a powerful tool for clinicians to assess functional limitations due to neurological or orthopedic conditions that are reflected in gait. Therefore, accurate gait monitoring and analysis methods have found a wide range of applications from diagnosis to treatment and rehabilitation. This thesis focuses on creating a low-cost and non-intrusive vision-based machine learning framework dubbed as iGait to accurately detect CLBP patients using 3-D capturing devices such as MS Kinect. To analyze the performance of the system, a precursor analysis for creating a feature vector is performed by designing a highly controlled in-lab simulation of walks. Furthermore, the designed framework is extensively tested on real- world data acquired from volunteer elderly patients with CLBP. The feature vector presented in this thesis show very high agreement in getting the pathological gait disorders (0.98% for in-lab settings and 90% for actual CLBP patients), with a thorough research on the contribution of each feature vector on the overall classification accuracy.

CHAPTER 2

Literature Review

2.1 Impact of health on gait

In an everyday environment the state of a person's health or even age can be determined by the way they walk also known as "gait". For example elderly people walks tend to walk slowly and tend to shuffle, while people with knee or hip injury tend to walk asymmetrically or drag their feet while walking. Several orthopedic and neurological disorders have shown their reflections on a patient's gait.

For example patients suffering from Type 2 Diabetes have effects in their stride frequency. People with preferred stride frequency(PSF) have their plantar pressure at the lowest level. The purpose of this study was to check how stride frequency above or below the preferred stride frequency affects the plantar loading. Their research suggested that the time to contact time and the pressure time while walking seems to be affected which results into plantar ulceration. [1].

Patients suffering from osteoarthritis also show some peculiar variations in their gait characteristics, more specifically their stride length. A study done by [2] where they included 102 patients for testing using functional assessment which includes analyzing the gait for 6 min walk. Stride characteristics were measured using the stride analyzer. Later they also discuss that with intervention, the group had an increase in 15% in walking distance as well as 9.1% increase in the stride length while free walking.

Neurological disorder like Parkinson's disease shows a direct relation to the abnormalities in stride length and stride frequency. [3] investigated to find out any relation between the abnormalities in the stride length-cadence relation in gait hypokinesia in Parkinson's

disease. In this study 20 patients were chosen and were instructed to walk a 10m track at cadence rates ranging from 40steps/min to 180steps/min. To guide the patients to maintain the cadence rate a metronome was used with the respective beat frequency. The gait patterns were recorded by a foot switch stride analyzer. Further linear regression analysis showed that the mean slope for the regression for stride length against cadence was not different for Parkinson's disease(PD) and normal patients but they showed a statistical difference in the mean intercept between the PD and control group.

Human gait has shown to be a strong indicator of health issues under a wide variety of conditions. For that reason, gait analysis has become a powerful tool for clinicians to assess functional limitations due to neurological or orthopedic conditions that are reflected in gait. Therefore, accurate gait monitoring and analysis methods have found a wide range of applications from diagnosis to treatment and rehabilitation [4], [5].

2.2 Data Acquisition Types

Studies for finding gait abnormalities have been divided into 2 cases:

1. Wearable sensor based methods
2. 3D Vision based methods

Wearable sensor based methods

The basic ideas for sensor based methods is to use physical sensors mounted on the subject's body to measure gait characteristics and later use some classification method to classify them. Sensors included for capturing these characteristics were as follows:

1. Inertial Measurement Unit (IMU)
2. Gyroscopes:
3. Capacitive Sensors
4. Force Sensitive Resistors

5. Markers on skin
6. Force Plates
7. BSN Sensor (Body Sensor Network)

Lower Body segments are usually considered for accelerometer/gyroscope placements to detect gait cycle events. For example [6] designed a system which could detect the four important phases of walks: stance, heel-off, swing, heel-strike. For this they used the gyroscope to measure the angular velocity of the foot and 3 force resistive resistors to get the forces exerted by the foot on the sole of the shoe by the person while walking. Despite walking either on regular, irregular or inclined surfaces the system could provide a very high reliability in detecting the walk phase for people with both normal and abnormal gait. This system also was unperturbed by any non-walking events such as weight shifting between legs during standing, feet sliding, sitting down and standing up.

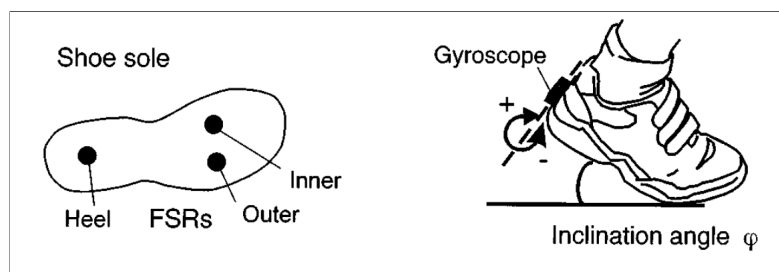


Figure 2.1: setup of 3 force resistive resistors(left) and a gyroscope(right), adopted from [6]

Another study by [7] gave evidence of utilizing accelerometers to get the spatio-temporal features for gait analysis. They based their hypothesis by utilizing a study done by [8] which stated that the three-dimensional displacements of the trunk can be well predicted by an inverted pendulum model of the body's center of mass trajectory. The amplitude and timing of pelvic displacements depended on the spatio-temporal parameters of the stride

cycle. Conversely the spatio-temporal parameters of the walk can be determined by the accelerations of the lower-trunk. Hence they checked the feasibility of this hypothesis where they placed an accelerometer at the lower trunk having sensitivity of 500mV/g and range: $\pm 2g$ and were able to prove that the system gave reliable results in identifying stride cycles for both left and right leg for overground walking and their system could provide a reliable methodology to test in real-time applications, however they cannot guarantee reliability if there were sharp turns while walking as the model was inspired from inverted pendulum model.

To reduce the number of intrusive sensors, since when we compare getting features from 2 limbs separately the user might feel uncomfortable. To tackle this problem [9] suggested that to get the accelerations of the lower trunk, one can place the sensors close to the L3 vertebral position. They got this inspiration after Zijlstra and Hof [7] who proved that the lower trunk accelerations and walking speed are similar for different subjects.

Similarly IMUs were used to detect the gait phases and features. The objective of the study was to classify gait abnormalities by using 3 IMUs (Opal, APDM, Inc., Portland, OR, USA) featuring a tri-axial accelerometer and a tri-axial gyroscope unit mass 22 g, unit size $48.5mm \times 36.5mm \times 13.5mm$, sampling frequency 128 Hz, accelerometer range $\pm 6g$, where $g = 9.81m/s^2$ were located on both shanks (about 20 mm above the malleoli with x, y and z axes pointing in vertical (VT, downward), antero-posterior (AP, forward) and medio-lateral (ML, right), directions respectively) and over the subject's lumbar spine, between L4 and S2, of each participant. [10]

Marker based technique was used by Nooriwati et. al[12] to create a classification system for Parkinson's disease. 12 healthy patients and 20 patients with Parkinson's disease were used for the test. 37 reflective markers were placed on the patient's body and then were tracked by using 6 infrared cameras placed at appropriate positions to ensure no loss of tracking of the tracker points. Also subjects were instructed to walk freely on two embedded

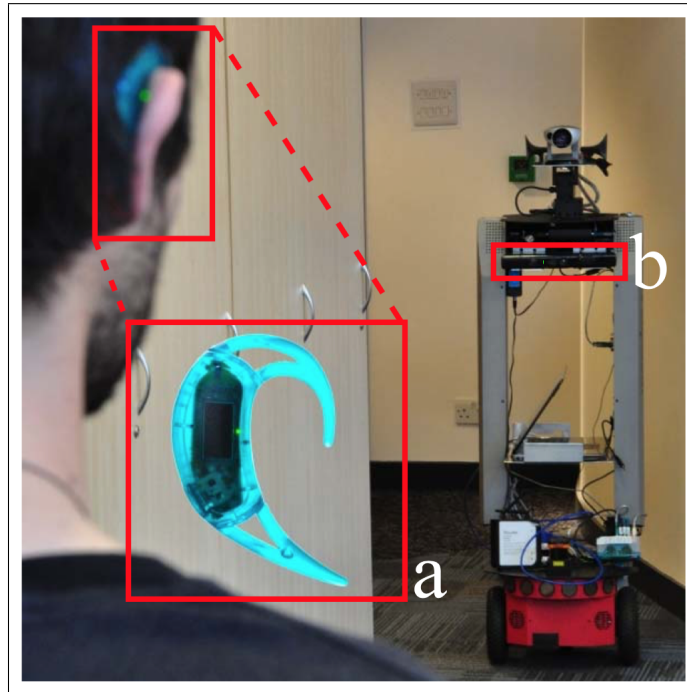


Figure 2.2: setup of a BSN sensor behind the ear and a RGB-D Camera, adopted from [11]

force plates where Ground Reaction Forces (GRFs) in all 3 directions (vertical, horizontal and lateral) were recorded, but while training only the vertical and horizontal forces were recorded. The camera was used to recorder the kinematic features(hip angle, knee angle, etc.) while the force plates were used to record the kinematic features(maximum vertical heel contact force, maximum horizontal push-off force, etc.)

In order to measure the stability or the risk of falling of a person [11] employed a Body Sensor Network(BSN) sensor that can be easily worn behind the ear and because of its lightweight property and wireless data transmission, it proves to be a viable solution for providing an unobtrusive sensing method. A BSN sensor has an embedded 3-axis accelerometer which ensures accumulation of data in a easy to wear and wireless fashion (fig. 2.2).This work was further extended by [13] to include depth camera which helped them in computing the body pose and leg separation as they proved to be also indicators of gait abnormality.

Vision Based sensors

For Vision based sensors, the methodology is usually divided into 2 parts.

1. *Model Based*: This approach usually employs fitting of a 3d model/skeleton to the RGB-D data and then later compute the gait features.

2. *Model Free*: Model free analysis usually utilizes the RGB data to create a silhouette over the body by first detecting a human body and then later getting relevant features from the silhouette.

An example of model free analysis used to recognize people based on their gait characteristics is proposed by Michela et. all [14]. They present a viewpoint independent, markerless system suitable for gait identification. Testing was done on 300 videos including surveillance and synthetic ones. The markerless system gave an accuracy of 92.5% for identifying people walking from different viewpoints based on their gait characteristics. This system proves to have a potential to be utilized in gait abnormality detection too.

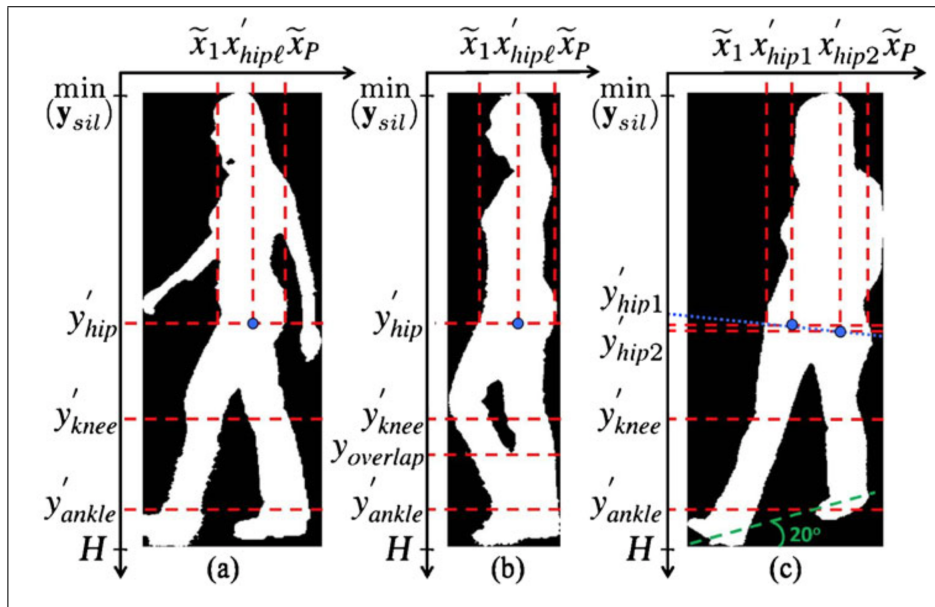


Figure 2.3: Computation of features at $\mu = 0$ with non-overlapping(a), overlapping(b) and at a viewpoint at $\mu = 20$ (c), adopted from [14]

In a model based system by using some detection algorithm a person is detected in a frame and then later a model (Can be a skeleton or a group of ellipses denoting limbs) is fit. Courtney et. all [15] created a novel system derived from spatiotemporal segmentation and model based tracking. The model used is an ellipse-based hierarchical tree structure. Once the outline has been is obtained and the body is segmented from the rest of the image, the outlines of the body formed by the snake's algorithm is then given to an ellipse-fitting algorithm, which then divides the body into ellipsoidal segments like head, torso, thigh and shank(fig.2.4). Once the fit is done, various gait features like knee flexion aple, tibial rotation, etc. are computed and will act as a precursor to detect gait abnormalities by using these features.

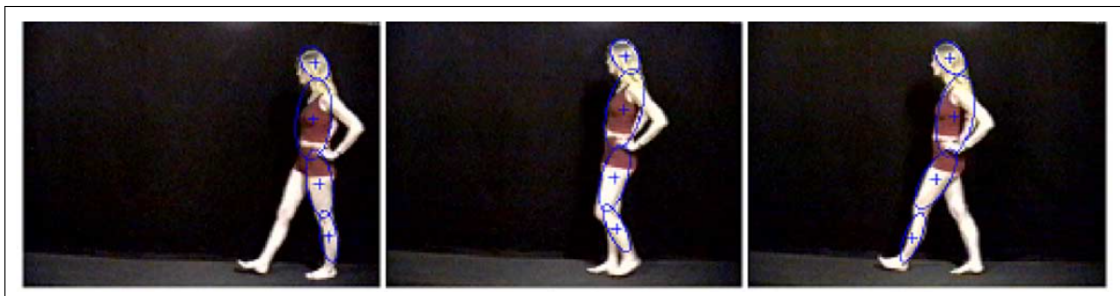


Figure 2.4: Individual ellipse model attached to the respective segments of the body, adopted from [14]

2.3 Chronic Low back pain

Recent studies reveal that over 26 million Americans suffer from Chronic Low Back Pain (CLBP) at least once a year resulting in substantial socio-economical impacts such as billions of dollars in medical costs and the cost of replacing the affected workforce during the long periods of high levels of pain [16], [17]. Moreover, elderly people are more prone to suffer from CLBP due to the health decline that is a result of aging which affects

neuromuscular function [18]. Detection of CLBP patients traditionally has been performed by X-rays, Magnetic Resonance Imaging (MRI) [19], and electromyography [20], [21]. Recently, a study was conducted to explore the capabilities of the accelerometer within a smart mobile environment [22] for classifying CLBP patients. Such intrusive methods are slow, expensive, and usually require the patient to be hospitalized under careful clinical supervision. The effects of CLBP on gait have long been studied and evaluated during the past decades [23], [24], [25]. More specifically, authors in [26], [27], and [23] attempted to classify deviations in gait patterns under CLBP. Consequently, detecting health decline by monitoring and analyzing gait over time is a crucial tool to prevent accidents or reduce the pain caused by CLBP.

CHAPTER 3

Methodology

The methodology section will be divided into

3.1 The iGait System

The architecture of the iGait system is illustrated in Fig. 3.1. iGait receives in input body-motion data from a body motion-capturing system, e.g., a low-cost depth camera (like Microsoft's Kinect) or a motion-capturing system. These data are transmitted by iGait, which processes them, extracts a feature vector and queries a trained classifier to classify the patient's likelihood to have a normal or abnormal walking pattern. If an abnormality is present, iGait extracts a recommendation to a user (e.g. healthcare expert) in the form of an alert notification. Our team has developed a web graphical-user interface (GUI) for notifying the medical expert and for providing him/her with a view of relevant body-motion parameters over a certain window of time.

The "Data Acquisition" block obtains patient's joints motion using a capturing device such as Kinect or any MOCAP. This data consist of a set of live measurements of the tri-dimensional (3-D) coordinates of the body joints at every frame. The capturing rate used in the experiments was 30 Hz.

These 3D joint coordinates are then passed to the "Feature Extraction" block (more details in Sect. 3.1.1). Note that, while in this paper we focus on extracting features to best recognize the onset of CLBP, any kind of spatio-temporal feature vectore could be extracted by this block to then train iGait to detect other medical conditions reflected in walking abnormalities (e.g., fall risk, Parkinson disease, etc.).

The features extracted at a short sequence of frames by the “Feature Extraction” block are used as inputs to the “Abnormality Classification” system, which outputs an abnormality identification (ID) for a particular time window over which the features were extracted. The presented system outputs two class labels, namely “normal” and “abnormal”. The “Abnormality Classification” system has been previously trained with features extracted from walking data with known labels. In case that an abnormal pattern has been detected, an alert message will be notified to the healthcare expert (e.g., via text message or any other means of communication considered in the iGait GUI).

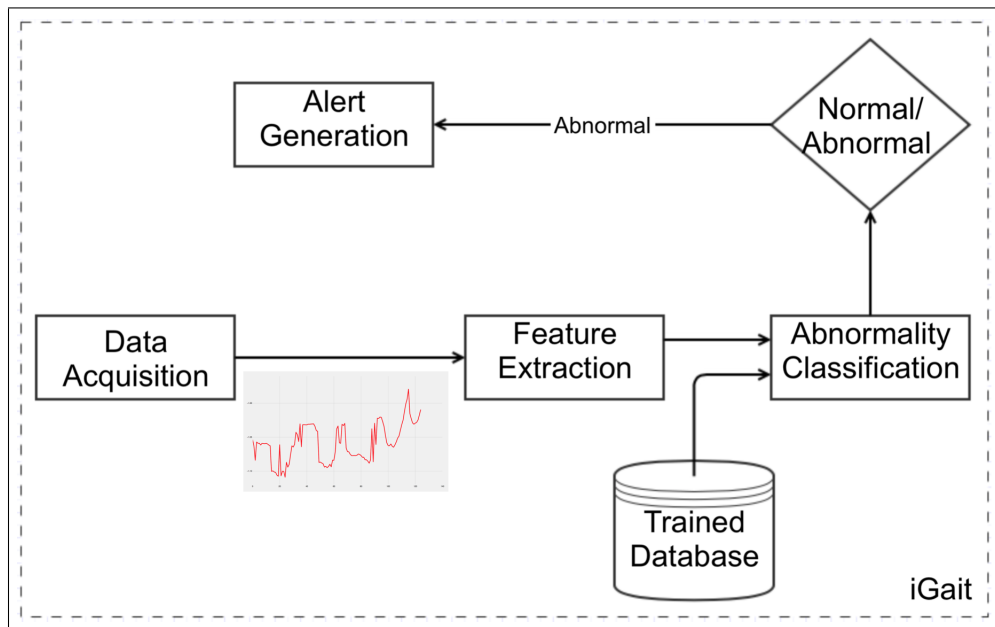


Figure 3.1: Block Diagram of iGait System

The Microsoft (MS) *KinectTMV1* captures the 3D scene information from its depth sensor. The sensor comprises of an infrared laser projector combined with a monochrome CMOS sensor, which captures video data in 3-D under any ambient light conditions. As visualized in Fig. 3.2 the device also has an RGB camera and a multi-array microphone for speech recognition [28]. The RGB camera in the middle of the device records image frames

with a resolution of 640x480 [29] pixels at a rate of 30 frames per second (fps). The depth sensor consists of an infrared projector (on the left) and an infrared camera (on the right) that uses the structured light principle [30] [31] to detect the distance of objects from the camera with a precision of 4–40 mm depending upon the distance from the sensor (usually from 0.5m until 4m).

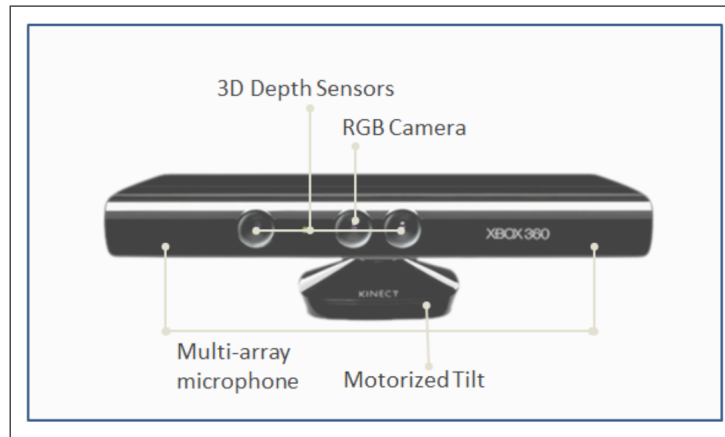


Figure 3.2: Kinect V1 Sensor [28]

On the other hand, the newer version of Kinect (known as Microsoft (MS) *KinectTM V2*) [32] has a higher RGB capture resolution of 1920x1080 pixels with a Time of Flight depth data as an image of resolution 512x424 resolution. The field of view for depth is 70 degrees horizontally and 60 degrees vertically [33].

In this paper, a Kinect V2 is used for acquisition since it tracks more joints and has a higher motion tracking accuracy, with greater stability.

The skeletal tracking tool included with the Kinect SDK V2 is utilized to collect the joint data. The Kinect device records the joints as points relative to the sensor itself. The joints that are obstructed cannot be resolved directly and are inferred from the rest of the posture of the person being tracked. The data was collected in frames where each frame

represents a posture of the person being tracked and it consists of 3-D coordinates of twenty five joints as shown in Fig. 3.3

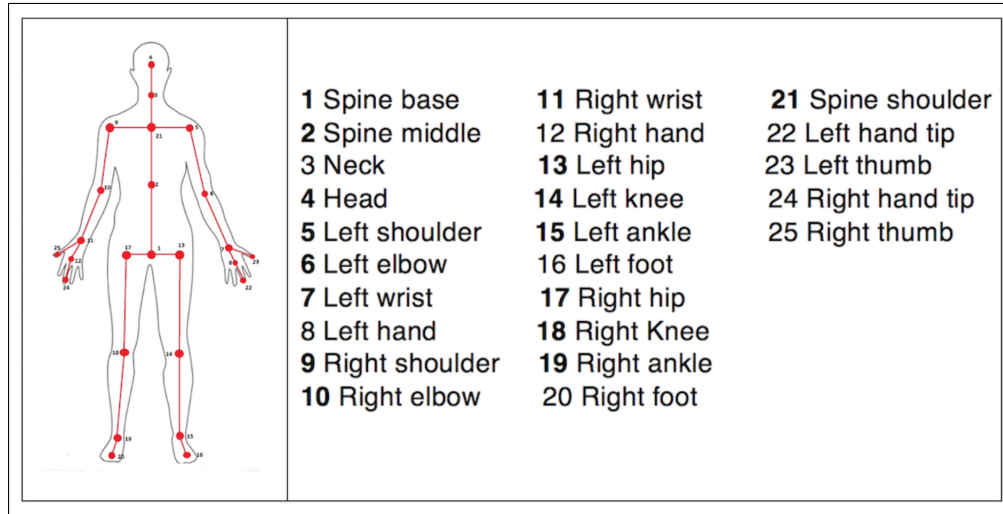


Figure 3.3: Kinect V2 Skeleton Map, adopted from [34]

For recognizing specific conditions of gait abnormalities (two abnormalities considered in this paper: CLBP and limping), selective joint positions were only taken into consideration in order to reduce computation complexity. The joint numbers highlighted in bold were considered for creating the features.

Preprocessing

Both the XYZ-positions and speeds of the aforementioned joints have a noise while they were recorded. In order to remove the noise, a second order low-pass Butterworth smoothing filter [35] based on the empirically-determined cutoff frequencies of 1Hz was used and it can be seen in the figure 3.4.

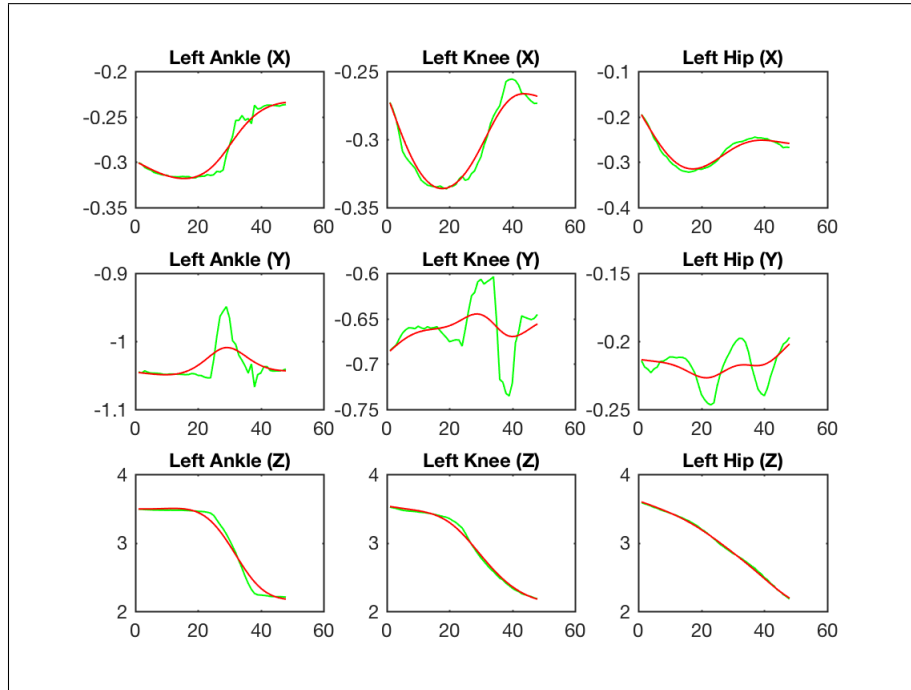


Figure 3.4: Kinect V2 Joints X,Y,Z co-ordinates in meters (green) with the filtered values(red)

Center of Mass Calculation

Based on the percentage weight distribution of different body segments, like head to neck, shoulder to forearm, neck to hip, hip to knee, knee to ankle and ankle to foot; individual segment Center Of Mass (COM) were calculated and the overall body's COM was their average.

Non-linear Curve Fitting

All the derived values obtained from the joint coordinates that were captured from the walks can be considered as time series and to extract meaningful features from such signals, a non-linear regression curve fitting was applied so that those model parameters can be used as features. We have used a model function comprising of sine and exponential component parameters to fit the time series data with the help of MATLAB's statistical and

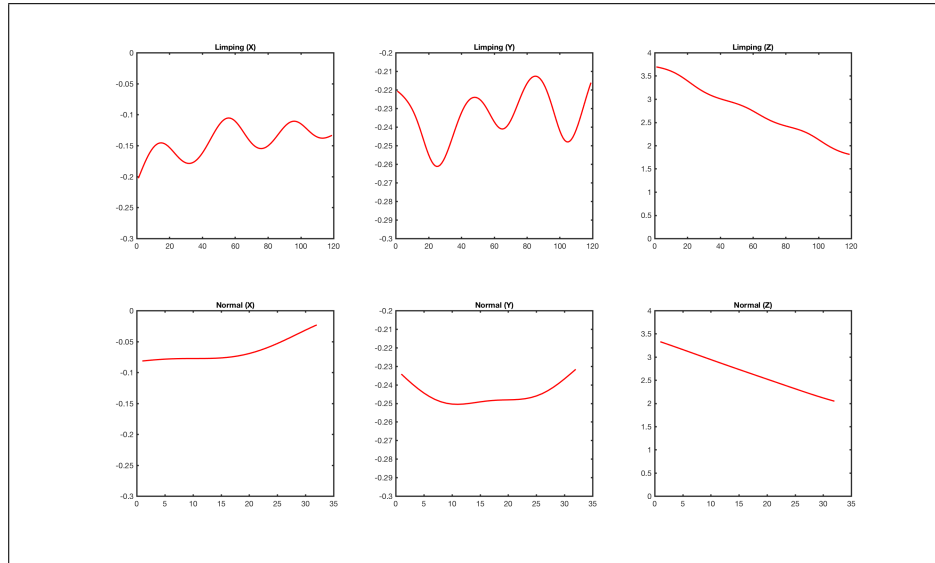


Figure 3.5: Computed Center of Mass X,Y,Z co-ordinates for Normal and Limping walk over number of frames

machine learning toolbox optimization functions and a subset of the estimated coefficients (amplitude and frequency) were used as features. This reduced the dimensionality of the features from n (number of frames) to 2.

3.1.1 Body Features Extraction

3.1.1.1 Hunch Angle

In a Propulsive gait condition, a person walks with a stooped stiff posture with head and neck bent forward. Propulsive gait characteristics are indicators of several gait disorders caused due to several medical conditions like Multiple Sclerosis, Parkinson's[6], etc. The hunch angle will quantify the extent a person is stooped forward while walking. It's the angle between the start of the spine joint (A), spine base (B) and the middle of feet (C), which is the average of the left and right ankle joints. The hunch angle for a video spanning for n number of frames is calculated as below,

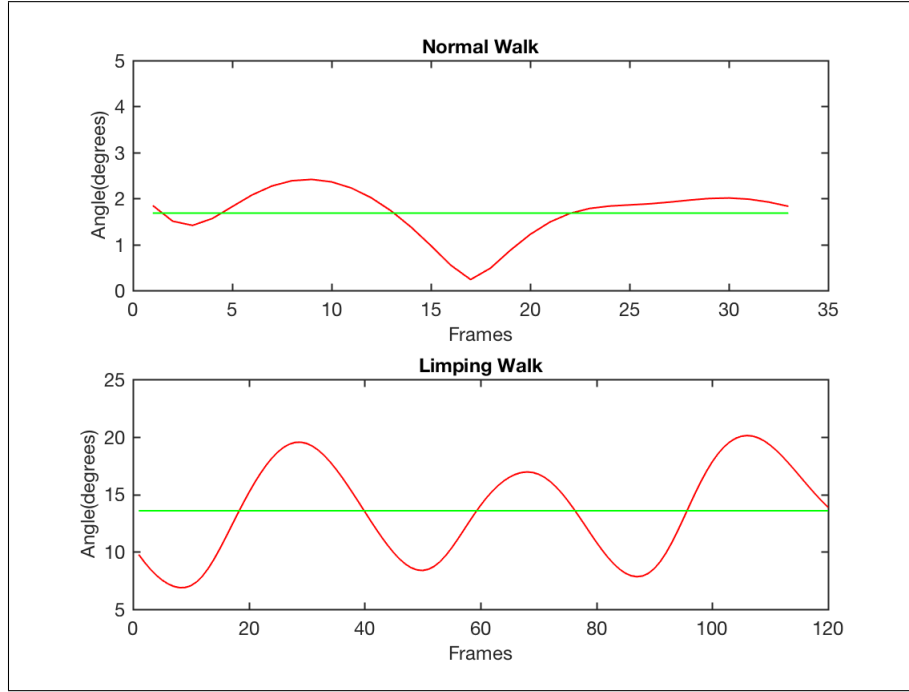


Figure 3.6: Hunch angles for normal and limping walks(Red indicates the actual data while green line indicates average)

$$\left\{ \begin{array}{l} \vec{AB} = A - B \\ \vec{BC} = B - C \\ \Theta_{hunch} = \frac{\sum_{i=1}^n \cos^{-1} \left(\frac{|\vec{AB}_i \cdot \vec{BC}_i|}{|\vec{AB}_i| |\vec{BC}_i|} \right)}{n} \end{array} \right. \quad (3.1)$$

3.1.1.2 Anterior and Mediolateral Angle

A good indicator for checking balance problems is to quantify the sway of upper body while walking [36]. Swaying either sideways or straight shifts the center of mass causing a disturbance in the overall walking rhythm which may result in fall. For this reason, we are calculating the anterior and mediolateral angles. The anterior angle(pitch) is the angle($\arctan 2$) between the Y and Z planes of the vector passing from the Center of mass

and the left ankle. The angle between the X and Z plane gives the mediolateral(roll) angle. Subsequently, the non-linear curve fitting explained in section 3.1 is employed to get the amplitude and frequency of these angles over time, which are then used as features. An example of the raw anterior and mediolateral angles (as measured by Kinect) are illustrated in Fig. 3.7 and Fig. 3.8 (red curve) while their least-squares fitting is showed in green.

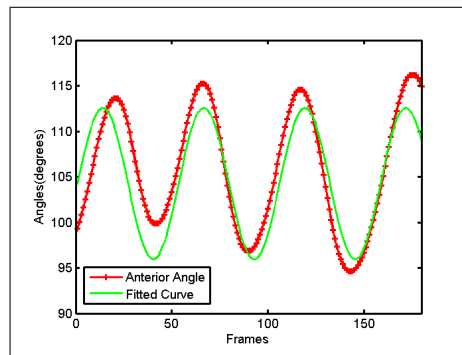


Figure 3.7: Anterior angle over a set of consecutive frames and the least square fitted curve.

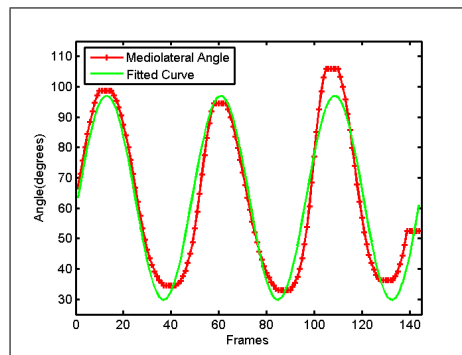


Figure 3.8: Mediolateral angle over a set of consecutive frames and the least square fitted curve

3.1.1.3 Knee angles (left and right leg)

Hemiplegic gait, primarily is a result of a cerebrovascular accident or stroke and is characterized by an extensor hypertonia in the lower limb causing a stiff movement of leg and reduced knee flexion in the swing phase[37]. To capture the kinematics of this abnormality and judge which side is hemiplegic, the knee angles of both legs were recorded while walking. The left and right knee angles were computed by using the angle between hip, knee and ankle joints of the respective sides. To extract the features of walking steps, the Z-component of the foot position[28] was used to segment the step phase and based on the frames when the feet were in the swing phase, knee angles of the respective leg were recorded and the mean and standard deviation of the angles of the individual legs were used as features.

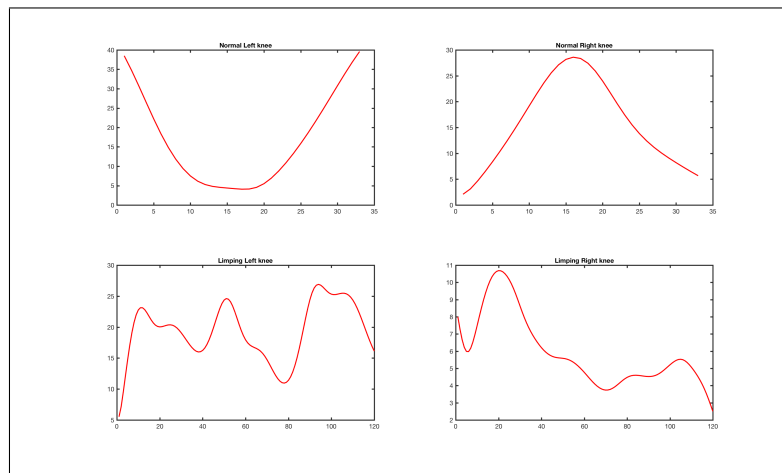


Figure 3.9: Knee angles for Left and Right leg for Limping and Normal walk.

3.1.1.4 Elbow angles (left and right leg)

Another peculiar characteristic of the hemiplegic gait is the development of flexor hypertonia in the upper limb, causing a stiffness in the elbow joint muscles resulting an

inability to swing the arms while walking [37]. The elbow angles were calculated by using the corresponding left or right hand using the 3 joints which are shoulder, elbow and wrist. The logic for angle computation is the same as that adopted for Hunch/Knee angle. (eq. 3.1).

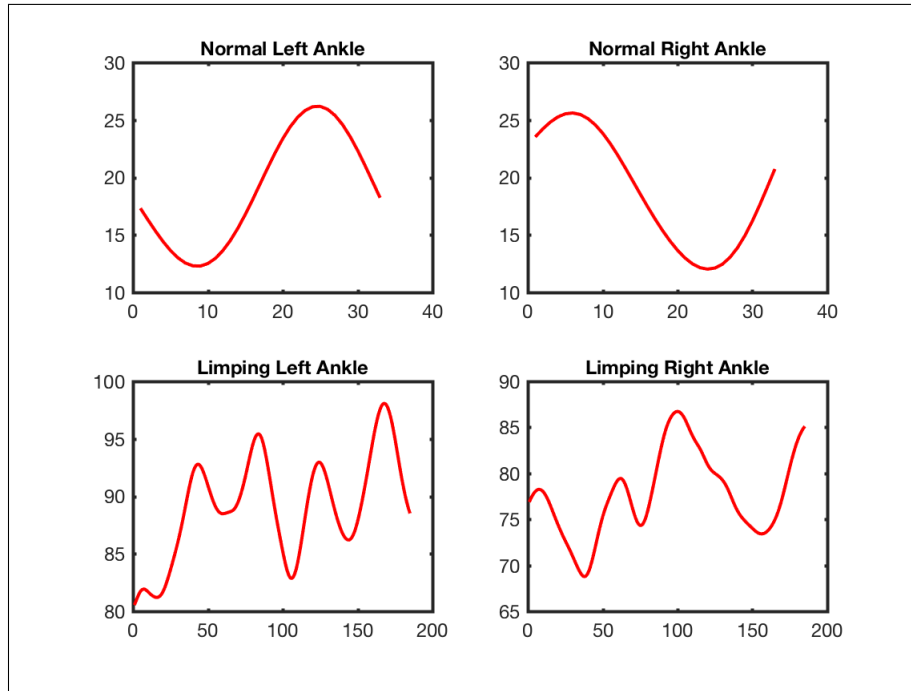


Figure 3.10: Elbow angles for Left and Right arms for Limping and Normal walk.

3.1.1.5 Left-Right leg Duration

Subjects suffering from Parkinson’s disease or having a diplegic gait[38] show a lot of adductor spasm in lower limbs resulting into little step walk and tend to drop their feet close towards the body while walking [39]. It can be inferred that during a phase of the walk, most of the time the legs might be close to each other and this time-dependent phenomenon can be extracted. Binarized Gradient with an empirically decided threshold for the difference between the left and right ankle’s positions computed over time gives us the knowledge

of the time where the two ankles were close to each other (Fig. 3.15). The sum of zeros normalized by the total number of frames were used as the features.

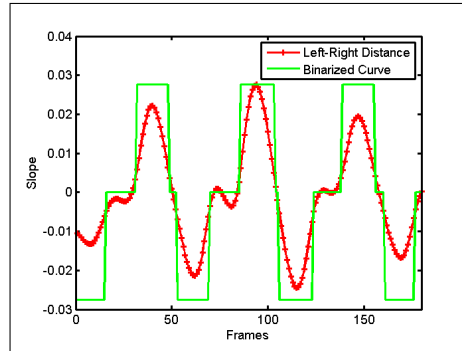


Figure 3.11: Gradient of difference of left and right ankle position and the corresponding binarized curve.

3.1.1.6 Knee Angle Wave

In Diplegic gaits[38], the patients show a universal flexion of joints more specifically for lower limbs, the relative variation of knee joint angle is very less. The difference between the angles of the left and the right knees were fed to the non-linear curve fitting to obtain the amplitude and frequency which in turn were used as features for classification(Fig. 3.12).

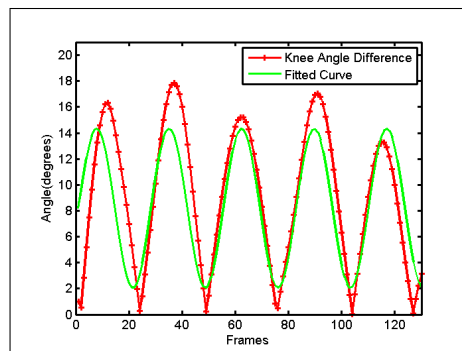


Figure 3.12: Knee angle difference and fitted curve.

3.1.1.7 Shoulder-Hip

Patients with chronic non-specific low back pain patients, walk with more synchronous (in-phase) horizontal pelvis and thorax rotations than controls[40]. The x component of left and right shoulder showed in-synchronicity for CLBP patients compared to normal patients(Fig. 3.13 and 3.14), so we measure this synchronicity by difference between the coordinates of the respective sides of shoulder and hip joint, which is then further subtracted from each other for each frame . Then a windowed maxima and minima is taken for each gait cycle and then mean, standard, deviation, range of these maxima and minima were used. Also a difference between the means of left shoulder to hip distance and right shoulder to hip distance is taken into consideration for the feature vector pool.

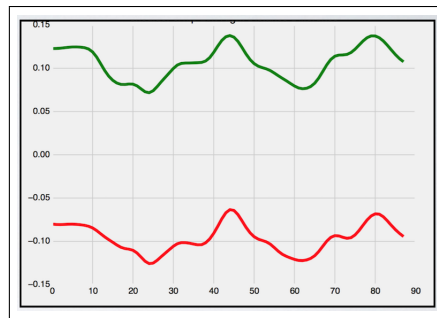


Figure 3.13: x component of left and right hip vs time for lowback pain patients

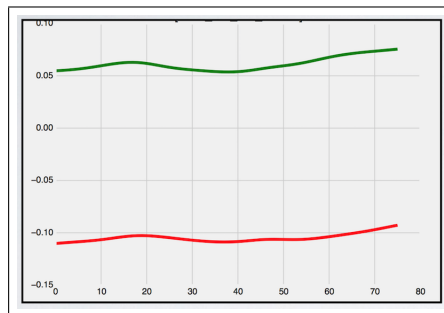


Figure 3.14: x component of left and right hip vs time for normal patients

3.1.1.8 Left-Right Distance (when feet closest and farthest)

To measure the stride length variability, we use the euclidean difference between the coordinates of the left and right ankle. The difference is then smoothed by running a rolling mean filter and then maxima and minima of the curve was calculated. The maximas will give us the frame locations where the distance between the feet were maximum, while minimas will give the locations where the distance between the feet were minimum. The respective mean of the maximas and minimas for multiple gait cycles were then normalized by the person's height which was calculated from the starting frames, when the person was standing stationery. The person's height was calculated by taking the average of difference of the y co-ordinate of head to both feet and averaged when the person was 4m away from kinect and stood upright.

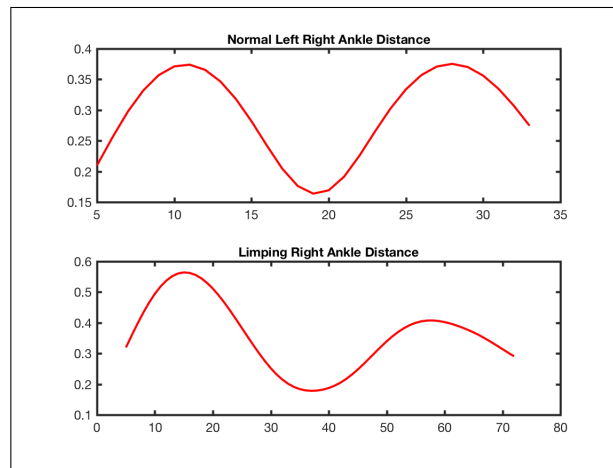


Figure 3.15: Difference between left and right ankle.

3.1.2 Fall Prediction

The overall fall-prediction algorithm is as shown in Fig. 3.16. It is comprised of 3 stages: *Capture*, *Process* and *Classify*. The *Capture* phase includes recording the 3-D joint

positions from the body via the Kinect SDK skeleton tracker. The recorded matrix will be of $N \times 25 \times 3$, where N stands for the number of frames, 25 are the number of joints and 3 are their respective X, Y and Z co-ordinates in Kinect's reference frame. The 3-D matrix is then passed to the Butterworth smoothing filter to filter out the noise. Furthermore, to remove the noisy beginning and ending of walk that happens due to being too far or too close to the sensor respectively, the step segmentation block is used.

The process phase includes the creation of feature vector for a recorded walk. The Center of mass block creates $N \times 3$ matrix based on the recorded joint positions. The create feature block utilizes this COM data along with the actual recorded 3-D joint position matrix to compute the feature vector. The feature vector is then finally normalized and fed to the classification block.

The classification model is responsible for generating an alert based on the given feature data. The classify sub-block gives us the classification gait abnormality category based on the new data fed to it with the help of a pre-trained model. Based on the classification result, the next block (Send SMS) decides to send an alert to the physician.

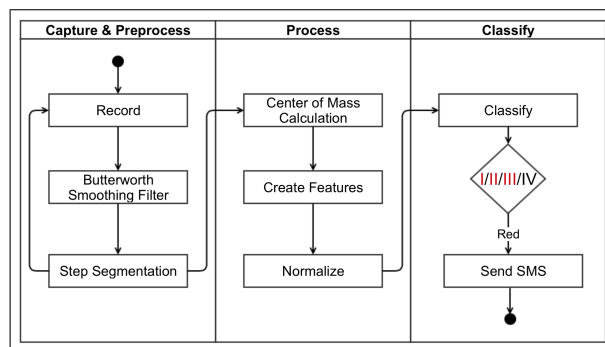


Figure 3.16: Flow diagram of Complete Algorithm.

Each subject was first asked to walk normally at three different speeds: habitual, slow and fast pace. Then a video was shown to make the subjects understand the way how a person walks if he was moderately limping because of discomfort in the left leg followed. A dry run test then followed. Similarly, the same procedure was done for moderate limping with a defect in the right leg. This was then performed with High level of limping for each leg. The whole experiment was first done with normal pace of limping, followed by high pace. Metronome was played to guide the volunteers for maintaining the stepping pace.

Numerical values indicate the number of videos taken for each subject (20 subjects were used in this in-lab validation study) while bold values stands for fast and underlined for slow pace of walking (Table. 3.1)

Pace	Non-Limping	Limping Type			
		Moderate		High	
Slow	3	<u>2</u>	2	<u>2</u>	2
Normal	3	<u>2</u>	2	<u>2</u>	2
Fast	3	<u>2</u>	2	<u>2</u>	2

Table 3.1: Count of video sequences for experiment

The features used for classification were *mediolateral angle, anterior angle, Left-Right distance, Knee angle difference, hunch angles, left and right knee angle with their means and standard deviations, mean left and right elbow angles*. A 10-fold cross-validation technique was used and 5 Nearest Neighbor [41], SVM classifier with linear and Gaussian Kernel [42] were adopted for classification.

Low-back pain patient data collection and testing

This study aims to create a machine learning framework for accurate detection of CLBP, to identify means so that they can walk with less difficulty. For the present study, patients suffering from low-back pain were recruited by a team of experts at Kinesiology department of University of Texas at Arlington. Patients with mild Low back pain were only considered so that they won't face problems while conducting the research. The local medical ethical committee approved the protocol and consent forms were provided to subject prior the recording. Additionally, to maintain the privacy of patients only skeletal depth data (no RGB) of the walks was recorded. Each person was first informed about the acquisition hardware, what the system aims at achieving and then they were instructed to start from a designated start point, walk straight towards the sensor at their natural pace and stop at a predefined marker about 0.5m away from Kinect. Bold markers were laid down on the floor to provide visual cues to help them to walk in straight line as well as act as an indicator for start and end position. A test run was done to make the patient get accustomed to the recording system.

In this study, we address the following concerns: 1) The accuracy of the proposed framework in detecting CLBP. 2) What subset of spatio-temporal features discussed in the literature are more suitable for such classification task. 3) Finally as part of the joint study with the Kinesiology department, we focussed on finding correlations between the extracted gait features and the amount of pain a subject perceives.

The inclusion criteria for patients was age between 50-75, male and female. There were in all 16 patients which were suffering from chronic back pain problems and 16 patients in the same age demographic with very little or no back-pain. The Kinesiology department was responsible to provide the ground truth data for the patients, which was decided by the team by making the patients perform many tests like Time Up and GO (TUG) as well as

brain mapping for getting the level of pain while performing some tasks and answering a sets of questionnaire.

Similar to the in-lab test, the setup was placed shown in Fig. 3.17. Each patient was told to walk towards the Kinect in a straight line at their natural pace for 6 times. The features extracted were the *mediolateral angle*, *anterior angle*, *Left-Right duration and normalized distance*, *Knee angle difference*, *hunch angles and Shoulder-Hip*. A 10-fold cross-validation technique was used and 5 Nearest Neighbor, Gaussian Mixture Model, and SVM classifier with linear and Gaussian Kernel were adopted for classification.

Recurrent Neural Networks (RNN) have been proven to be useful to find dependencies and pattern over the length of a signal. Additionally, using self-loops to produce paths where the gradient can flow for long duration is a core contribution of the initial Long short-term memory (LSTM) model[43]. By making the the weight of the self-loop gated and controlled by another hidden unit, the time scale of integration can be dynamically changed [44]. In order to classify walks using neural networks, a sequence database was created and statistically normalized using individual mean and standard deviations. 3D joint coordinates for all of the 25 joints were used for training and classification. First 60 frames starting from the initiation of the walk were used per sample. An LSTM unit with input size of 75 corresponding to $(25 * 3)$ 3D joint coordinates with a hidden size of 64 was used while the output of it was fed to a fully connected network and finally a logsoftmax layer.

CHAPTER 4

Experimental Results

4.1 Experimental Results

Graphical User Interface: The experiments consist of a simulated in-lab test and a real-world test on CLBP patients in collaboration with the kinesiology department. In order to facilitate data acquisition and analysis of these experiments, an easy to use and efficient GUI was developed in MATLAB (Fig. 4.1). The GUI includes online and offline analysis and classification functionality for live and pre-recorded walks. A record button invokes the Kinect Skeleton tracker developed in C++ which utilizes the SDK for Kinect V2 for real-time data acquisition of the 3D skeleton joints. Additionally, Classify Walk button, processes the previously recorded walks from the database for classification and visualizes the raw data. The graphical interface provides the user the flexibility to select the type of the classifier for the recorded walk. Furthermore, to provide more accurate information to the user, the lower left sub-window will show the raw data acquired by the tracker in the form of a skeleton scaled appropriately, while the lower right window gives the raw X, Y and Z co-ordinates of the center of mass.

For in-lab experiments, the results are visualized on the plot by means of highlighting the respective leg joints (blue color) which had abnormal movement as shown in Fig. 4.2.

4.1.1 Classification metrics

In order to avoid domination of some features for the overall classification, the features were normalized to range $[1, -1]$ appropriately. SVM was also included along-with 5 neighborhood KNN, due to its high accuracy and ability to work optimally with high

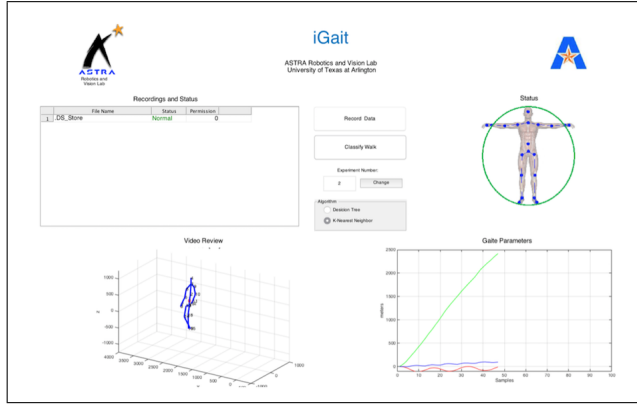


Figure 4.1: MATLAB GUI for recording and classification

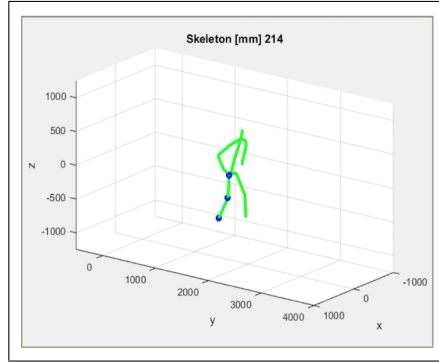


Figure 4.2: Right leg joints highlighted in blue

dimensional data [45]. For using SVM classifier, the library libSVM [46] was adopted. For choosing the optimal parameters to get the highest accuracy for SVM model training, a script supplied by LibSVM was used which first applies a coarse grid search to find a good combination of C and γ values and then a fine grid search to find the optimal set of parameter values. This value is used for the k-fold cross-validation and generating the metrics as shown in table 1.

Recall (or Sensitivity or true positive rate) measures the coverage of real positive cases by the predicted positive rule[47]. In our context it will stand for how the classifier performs in identifying all positive cases and it's a part of a holistic analysis, called ROC.

$$Recall = sensitivity = tpr = \frac{TP}{RP} = \frac{TP}{TP + FN}$$

TP represents the true positives the classifier could successfully detect in all real positives(RP) pool, which comprises of TP and false negatives(FN). On the other hand, FN represents those cases in which the classifier misclassified them as negatives.

Precision or confidence conversely determines the proportion of predicted positive cases that are correctly real positives[47]. Compared to tpr, which is a measure of rate of discovering real positives, precision or true positive accuracy(tpa) is a measure of accuracy of predicted positives [47].

$$Precision = tpa = \frac{TP}{PP} = \frac{TP}{TP + FP}$$

FP are the cases the classifier misclassified them as positives. F-measure combines the precision and recall and is a harmonic mean of the two. Accuracy is the measure of how the classifier could detect true negatives(TN) and true positives(TP) out of all results.

$$Accuracy = (TP + TN) / (TP + FP + FN + TN)$$

Classifier	Accuracy	Precision	F-score	Recall
5-NN	0.96	0.96	0.96	0.97
Linear SVM	0.97	0.97	0.97	0.96
Gaussian SVM	0.98	0.98	0.98	0.98

Table 4.1: Classification metrics for in-lab experiments

Based on the experimental setup and the classification strategy explained in section 3.2b and 3c, the classification performance for the in-lab test results are tabulated in Table 4.1. We found that the highest accuracy and recall was achieved by Gaussian SVM(RBF) Kernel since it can perform better in case of non-linear separation between classes. [48].

For the low-back pain test, we have used 5 neighborhood KNN, SVM and Gaussian mixture model (GMM). For SVM, the tuning parameters were obtained with the same

strategy as that of in-lab test. For Gaussian Mixture Model, a "spherical" covariance type was used to constrain the covariance of the different estimated classes. Using the same 10-fold cross-validation strategy and with a richer feature set compared to the in-lab tests, the classification metrics (Table 4.2) was obtained. LSTM with zero knowledge of feature vector gave the highest accuracy, which proves a viable solution for future.

Classifier	Accuracy	Precision	F-score	Recall
5-NN	0.77	0.80	0.75	0.77
Linear SVM	0.87	0.89	0.89	0.89
Gaussian SVM	0.86	0.88	0.86	0.87
GMM	0.86	0.87	0.87	0.87
LSTM	0.90	0.92	0.89	0.90

Table 4.2: Classification metrics for Low-back pain patients

4.1.2 Feature Significance

To find the impact of each feature for classification accuracy, we did a feature significance test using a forest of trees utility provided by sklearn [49]. A meta estimator was used which includes 100 randomized decision trees that ran on several subsamples of the features producing the plots for in-lab testing (Fig. 4.3) and low-back pain(Fig. 4.4), where the red bars signifies the feature importance while the blue line signifies the inter-tree variability. The x axis represents the feature indices used in the classification, while the y-axis is the feature importance percentage. Note that the features which have low ranking doesn't mean that they are not all unimportant, it just means they are correlated with each other a lot and either can be substituted with other of similar ranking.

<i>Index</i>	<i>Feature Name</i>	<i>Feature Description</i>
0	Left-Right Duration	Average time feet are close to each other in each step
1	Mediolateral Amplitude	Amplitude of the Sine curve fitted to Mediolateral angle signal
2	Mediolateral Frequency	Frequency of the Sine curve fitted to Mediolateral angle signal
3	Anterior Amplitude	Amplitude of the Sin curve fitted to Anterior angle signal
4	Anterior Frequency	Frequency of the Sin curve fitted to Anterior angle signal
5	Knee Amplitude	Amplitude of the Sin curve fitted to Knee angle signal
6	Knee Frequency	Frequency of the Sin curve fitted to Knee angle signal
8	Left-Right Least Distance	Height normalized local minima's mean of left-right ankle difference
9	Left-Right Great Distance	Height normalized local maxima's mean of left-right ankle difference
10	Shoulder-Hip Min Median	Average of local minimas for shoulder-hip difference signal
11	Shoulder-Hip Min Std	Standard deviation of local minimas for shoulder-hip difference signal
12	Shoulder-Hip Min Range	Range of local minimas for shoulder-hip difference signal

Table 4.3: List of features used in the experiments and their respective indices used in Fig. 4.3 and 4.4.

<i>Index</i>	<i>Feature Name</i>	<i>Feature Description</i>
13	Shoulder-Hip Max Mean	Mean of local maximas for shoulder-hip difference signal
14	Shoulder-Hip Max Median	Average of local maximas for shoulder-hip difference signal
15	Shoulder-Hip Max Std	Standard deviation of local maximas for shoulder-hip difference signal
16	Shoulder-Hip Max Range	Range of local maximas for shoulder-hip difference signal
17	Shoulder-Hip Max-Min	Difference of mean of difference between local maximas and minimas for shoulder-hip difference signal

Table 4.4: List of features used in the experiments and their respective indices used in Fig. 4.3 and 4.4(Continued).

Referring the feature importance rankings for in-lab experiments, where the classes were left-leg limping, right-leg limping, wide walk and normal walk, it can be confirmed that left right distance, which signified the time for which both the ankles were close to each other, where a person usually faces discomfort to extend the leg completely and hence lands the quickly near the other, captured the essence of limping, while second and third ranked mediolateral angles played a very important role in classification, since the visualization of these walks showed significant sway of the spine sideways. Only considering the top 5 features we could achieve an accuracy as show in the below classification metrics for the in-lab tests(Table 4.6).

Rankings for the low-back pain showed expected results, which had top 2 from the shoulder to hip features, which are the primary indicators for low-back pain patients, since their walks showed an unusual constricted/unsynchronized hip movements. Only

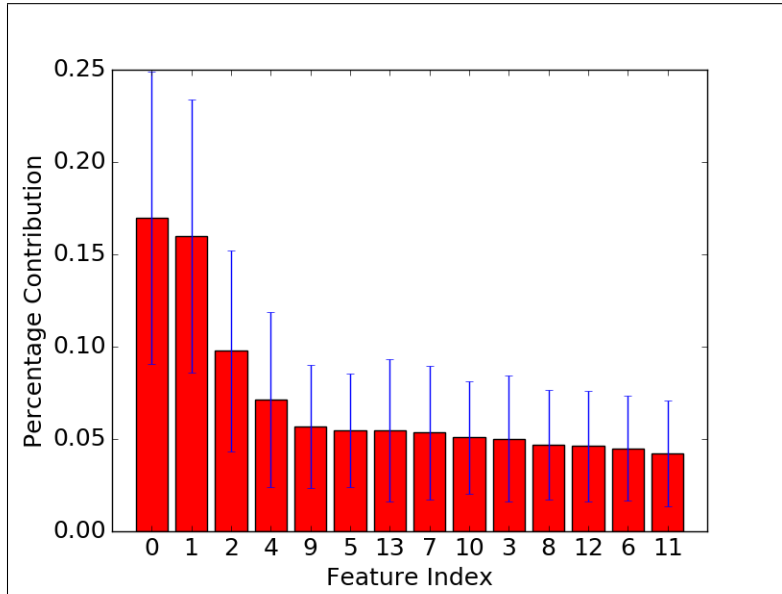


Figure 4.3: Feature importance for in-lab experiment

Classifier	Accuracy	Precision	F-score	Recall
5-NN	0.87	0.85	0.85	0.85
Linear SVM	0.76	0.77	0.76	0.77
Gaussian SVM	0.82	0.83	0.82	0.82

Table 4.5: Metrics (top 5 features) for in-lab experiments

considering the top 5 features we could achieve an accuracy as show in the classification metrics(Table 4.6) for the low-back pain tests.

Classifier	Accuracy	Precision	F-score	Recall
5-NN	0.77	0.77	0.78	0.77
Linear SVM	0.75	0.75	0.75	0.75
Gaussian SVM	0.75	0.76	0.76	0.75
GMM	0.67	0.68	0.65	0.68

Table 4.6: Metrics (top 5 features) for low-back pain experiments

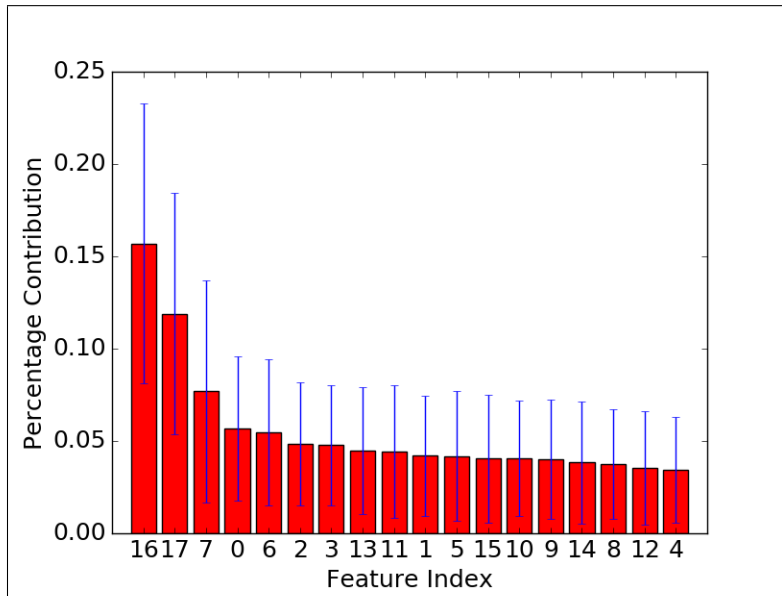


Figure 4.4: Feature importance for Low-back pain experiment

4.1.3 ROC Curves

In-lab Test

For computing the ROC for in-lab tests the multiclass (limping left, limping right, wide walk and normal) classification problem was modified into a binary one vs all classification problem which resulted into 4 different ROCs for each class. The class labels previously labelled as (0/1/2/3), which was a $N \times 1$ vector was binarized to [1000], [0100], [0010] and [0001] respectively making it to a $N \times 4$ vector. Now to compute the ROC for i th class the i th column class label was considered as class label, which in turn turned the problem into a binary classification one. The ROC for class label "non-limping" (class index = 0) is as follows (Fig. 4.5)

Referring to Fig. 4.5, the Area under the curve for normal walk for KNN was the highest.

The ROC for class label "limping left" (class index = 1) is as shown in Fig. 4.6. The Area under the curve for limping left class for KNN and SVM Linear Kernel was the highest.

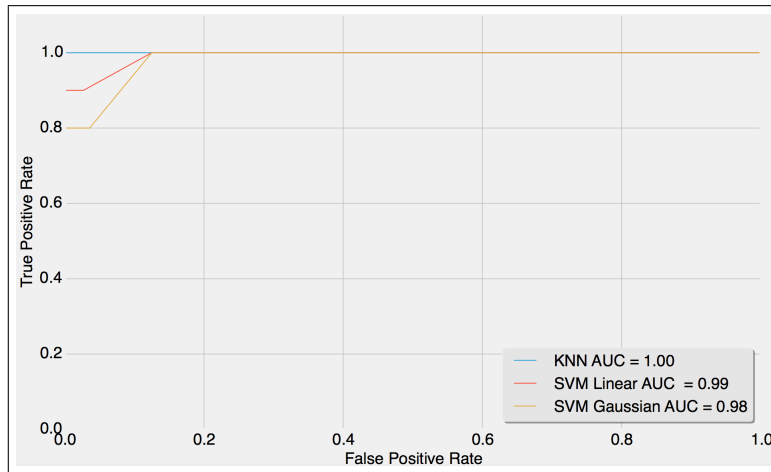


Figure 4.5: ROC for Class Index 0

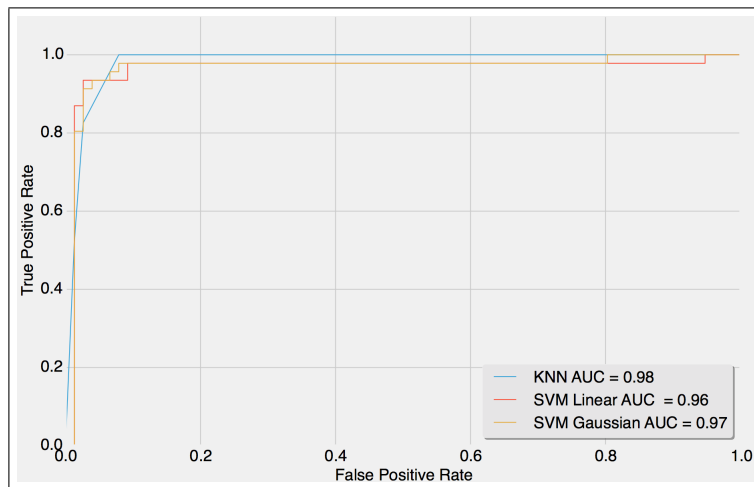


Figure 4.6: ROC for Class Index 1

The ROC for class label "limping right" (class index = 2) is as shown in Fig. 4.7, the Area under the curve for limping right class for KNN was the highest.

The ROC for class label "wide walk" (class index = 3) shown in Fig. 4.8, the Area under the curve for wide walk class for was the highest using any classifiers.

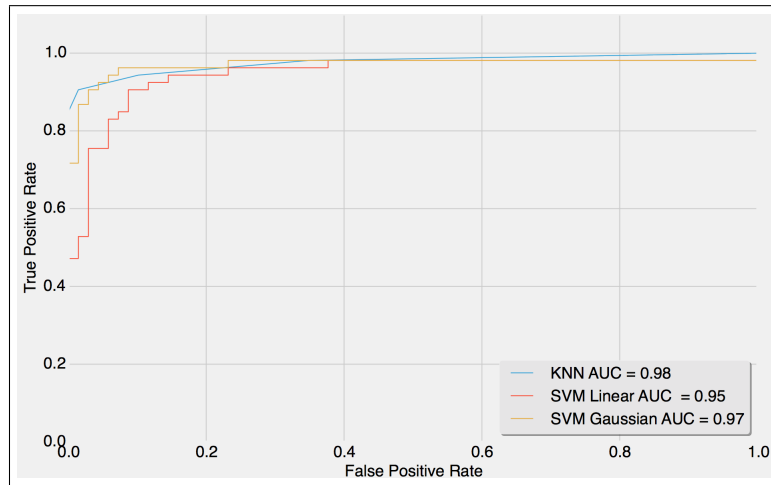


Figure 4.7: ROC for Class Index 2

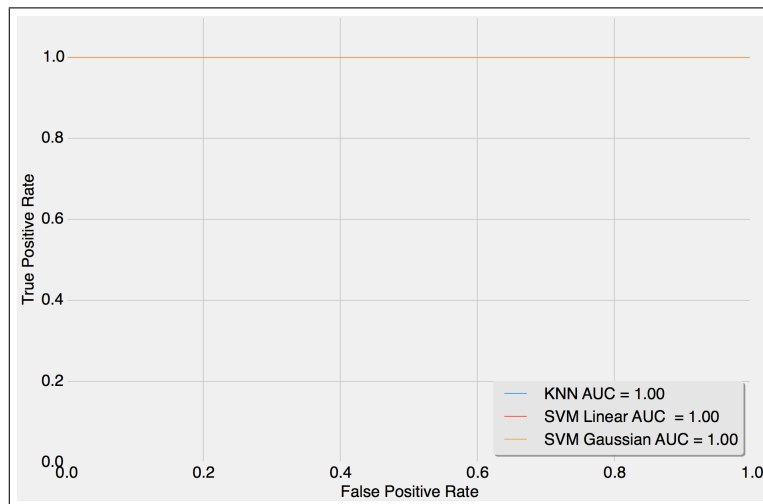


Figure 4.8: ROC for Class Index 3

low back pain Test

Similar analysis was used to plot the ROC for low back pain classes. The Area under the curve (AUC) is effective and is a combined estimate of sensitivity and specificity that describes the validity of diagnostic test. As shown in the figure (fig 4.9), SVM with Gaussian Kernel is having the highest area under the curve i.e. it will be able to distinguish a person having low-back pain or not very efficiently compared to other classifiers.

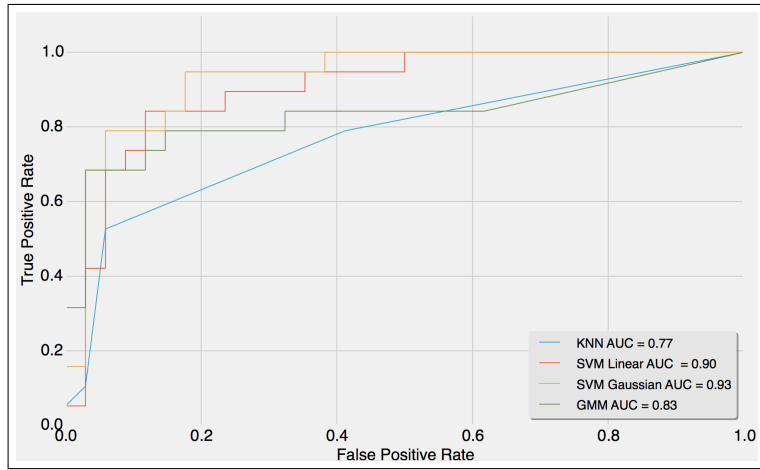


Figure 4.9: ROC for low back pain Class

CHAPTER 5

Conclusion and Future Work

5.1 Conclusion and Future Work

By leveraging Kinect V2, which provides a low-cost, non-contact and accurate gait capturing system, this machine learning framework can be used to effectively detect low-back pain . The methodology includes capturing and filtering of the data to ensure an accurate acquisition of spatio-temporal data and then by formulating a set of reliable features which was created by a 2-step procedure, one in the lab and then later fine tuning it to test it with the real-life patients a reliable and non-intrusive system was developed to accurately classify low-back pain patients. For the in-lab tests, where the skeleton was synthetically produced using 20 participants, enabled to test our initial validation of the feature set which was primarily inspired by understanding the motion of human body. The ROC curves prove that the system was highly accurate to not misclassify someone with a normal walk. The logic when tested with real-life patients resulted in a lower accuracy, but due to the flexibility of the machine learning framework, new gait abnormality specific features were easily included in the pool and the system could achieve a maximum of 90% classification accuracy for the real patients.

In future one can apply this framework to detect other gait abnormalities by modifying the feature set. Also LSTM proved to be a viable solution for future research since it was able to provide the maximum accuracy without prior knowledge of feature vector and only using the raw 3d co-ordinates from kinect it was able to find dependencies over the video sequence.

REFERENCES

- [1] A. Bellmeyer and J. Strasser, “Effect of stride frequency on plantar loading in type 2 diabetes.”
- [2] M. Peterson, P. Kovar-Toledano, J. Otis, J. Allegrante, C. Mackenzie, B. Gutin, and M. Kroll, “Effect of a walking program on gait characteristics in patients with osteoarthritis,” *Arthritis & Rheumatology*, vol. 6, no. 1, pp. 11–16, 1993.
- [3] M. Morris, R. Ianseck, T. Matyas, and J. Summers, “Abnormalities in the stride length-cadence relation in parkinsonian gait,” *Movement Disorders*, vol. 13, no. 1, pp. 61–69, 1998.
- [4] M. Gabel, R. Gilad-Bachrach, E. Renshaw, and A. Schuster, “Full body gait analysis with kinect,” in *Engineering in Medicine and Biology Society (EMBC), 2012 Annual International Conference of the IEEE*. IEEE, 2012, pp. 1964–1967.
- [5] D. HODGINS, “The importance of measuring human gait,” *Medical Device Technology*, vol. 19, no. 5, 2008.
- [6] I. P. Pappas, M. R. Popovic, T. Keller, V. Dietz, and M. Morari, “A reliable gait phase detection system,” *IEEE Transactions on neural systems and rehabilitation engineering*, vol. 9, no. 2, pp. 113–125, 2001.
- [7] W. Zijlstra and A. L. Hof, “Assessment of spatio-temporal gait parameters from trunk accelerations during human walking,” *Gait & posture*, vol. 18, no. 2, pp. 1–10, 2003.
- [8] —, “Displacement of the pelvis during human walking: experimental data and model predictions,” *Gait & posture*, vol. 6, no. 3, pp. 249–262, 1997.

- [9] R. C. González, A. M. López, J. Rodríguez-Uría, D. Álvarez, and J. C. Alvarez, “Real-time gait event detection for normal subjects from lower trunk accelerations,” *Gait & posture*, vol. 31, no. 3, pp. 322–325, 2010.
- [10] A. Mannini, D. Trojaniello, A. Cereatti, and A. M. Sabatini, “A machine learning framework for gait classification using inertial sensors: application to elderly, post-stroke and huntington’s disease patients,” *Sensors*, vol. 16, no. 1, p. 134, 2016.
- [11] R. C. King, L. Atallah, C. Wong, F. Miskelly, and G.-Z. Yang, “Elderly risk assessment of falls with bsn,” in *Body Sensor Networks (BSN), 2010 International Conference on*. IEEE, 2010, pp. 30–35.
- [12] N. M. Tahir and H. H. Manap, “Parkinson disease gait classification based on machine learning approach,” *Journal of Applied Sciences*, vol. 12, no. 2, p. 180, 2012.
- [13] C. Wong, S. McKeague, J. Correa, J. Liu, and G.-Z. Yang, “Enhanced classification of abnormal gait using bsn and depth,” in *Wearable and Implantable Body Sensor Networks (BSN), 2012 Ninth International Conference on*. IEEE, 2012, pp. 166–171.
- [14] M. Goffredo, I. Bouchrika, J. N. Carter, and M. S. Nixon, “Performance analysis for automated gait extraction and recognition in multi-camera surveillance,” *Multimedia Tools and Applications*, vol. 50, no. 1, pp. 75–94, 2010.
- [15] J. Courtney and A. M. De Paor, “A monocular marker-free gait measurement system,” *IEEE Transactions on neural systems and rehabilitation engineering*, vol. 18, no. 4, pp. 453–460, 2010.
- [16] T. A. Mattei, A. A. Rehman, A. R. Teles, J. C. Aldag, D. H. Dinh, and T. D. McCall, “The ‘lumbar fusion outcome score’(lufos): a new practical and surgically oriented grading system for preoperative prediction of surgical outcomes after lumbar spinal fusion in patients with degenerative disc disease and refractory chronic axial low back pain,” *Neurosurgical review*, vol. 40, no. 1, pp. 67–81, 2017.

- [17] B. I. Martin, R. A. Deyo, S. K. Mirza, J. A. Turner, B. A. Comstock, W. Hollingworth, and S. D. Sullivan, "Expenditures and health status among adults with back and neck problems," *Jama*, vol. 299, no. 6, pp. 656–664, 2008.
- [18] L. Donath, O. Faude, E. Lichtenstein, G. Pagenstert, C. Nüesch, and A. Mündermann, "Mobile inertial sensor based gait analysis: Validity and reliability of spatiotemporal gait characteristics in healthy seniors," *Gait & Posture*, vol. 49, pp. 371–374, 2016.
- [19] T. Dillingham, "Evaluation and management of low back pain: an overview," *SPINE-PHILADELPHIA-HANLEY AND BELFUS-*, vol. 9, pp. 559–596, 1995.
- [20] C. T. Candotti, J. F. Loss, A. M. S. Pressi, F. A. de Souza Castro, M. La Torre, M. de Oliveira Melo, L. D. Araújo, and M. Pasini, "Electromyography for assessment of pain in low back muscles," *Physical therapy*, vol. 88, no. 9, p. 1061, 2008.
- [21] M. E. Geisser, M. Ranavaya, A. J. Haig, R. S. Roth, R. Zucker, C. Ambroz, and M. Caruso, "A meta-analytic review of surface electromyography among persons with low back pain and normal, healthy controls," *The journal of pain*, vol. 6, no. 11, pp. 711–726, 2005.
- [22] H. Chan, H. Zheng, H. Wang, and D. Newell, "Assessment of gait patterns of chronic low back pain patients: A smart mobile phone based approach," in *Bioinformatics and Biomedicine (BIBM), 2015 IEEE International Conference on*. IEEE, 2015, pp. 1016–1023.
- [23] L. Arendt-Nielsen, T. Graven-Nielsen, H. Svarrer, and P. Svensson, "The influence of low back pain on muscle activity and coordination during gait: a clinical and experimental study," *Pain*, vol. 64, no. 2, pp. 231–240, 1996.
- [24] Y. Barzilay, G. Segal, R. Lotan, G. Regev, Y. Beer, B. S. Lonner, A. Mor, and A. Elbaz, "Patients with chronic non-specific low back pain who reported reduction in pain and improvement in function also demonstrated an improvement in gait pattern," *European Spine Journal*, vol. 25, no. 9, pp. 2761–2766, 2016.

- [25] M. Mazaheri, P. Coenen, M. Parnianpour, H. Kiers, and J. H. van Dieën, “Low back pain and postural sway during quiet standing with and without sensory manipulation: a systematic review,” *Gait & posture*, vol. 37, no. 1, pp. 12–22, 2013.
- [26] F. J. Keefe and R. W. Hill, “An objective approach to quantifying pain behavior and gait patterns in low back pain patients,” *Pain*, vol. 21, no. 2, pp. 153–161, 1985.
- [27] R. Fernandes, A. Pool-Goudzwaard, V. M. Pereira, P. A. da Silva, and A. P. Veloso, “Loss of variability and altered three-dimensional trunk and hip kinetics during gait in chronic low back pain individuals,” *Faculdade de Motricidade Humana*, p. 59, 2016.
- [28] M. Parajuli, D. Tran, W. Ma, and D. Sharma, “Senior health monitoring using kinect,” in *Communications and Electronics (ICCE), 2012 Fourth International Conference on*. IEEE, 2012, pp. 309–312.
- [29] A. Procházka, O. Vyšata, M. Vališ, O. Āupa, M. Schätz, and V. Mařík, “Use of the image and depth sensors of the microsoft kinect for the detection of gait disorders,” *Neural Computing and Applications*, vol. 26, no. 7, pp. 1621–1629, 2015.
- [30] K. Khoshelham and S. O. Elberink, “Accuracy and resolution of kinect depth data for indoor mapping applications,” *Sensors*, vol. 12, no. 2, pp. 1437–1454, 2012.
- [31] S. Qin, X. Zhu, Y. Yang, and Y. Jiang, “Real-time hand gesture recognition from depth images using convex shape decomposition method,” *Journal of Signal Processing Systems*, vol. 74, no. 1, pp. 47–58, 2014.
- [32] J. Steward, D. Lichti, J. Chow, R. Ferber, and S. Osis, “Performance assessment and calibration of the kinect 2.0 time-of-flight range camera for use in motion capture applications,” *FIG Working Week 2015*, pp. 1–14, 2015.
- [33] E. Lachat, H. Macher, M. Mittet, T. Landes, and P. Grussenmeyer, “First experiences with kinect v2 sensor for close range 3d modelling,” *The International Archives of Photogrammetry, Remote Sensing and Spatial Information Sciences*, vol. 40, no. 5, p. 93, 2015.

- [34] A. P. Rocha, H. Choupina, J. M. Fernandes, M. J. Rosas, R. Vaz, and J. P. S. Cunha, “Kinect v2 based system for parkinson’s disease assessment,” in *Engineering in Medicine and Biology Society (EMBC), 2015 37th Annual International Conference of the IEEE*. IEEE, 2015, pp. 1279–1282.
- [35] J. Zhao, F. E. Bunn, J. M. Perron, E. Shen, and R. S. Allison, “Gait assessment using the kinect rgb-d sensor,” in *Engineering in Medicine and Biology Society (EMBC), 2015 37th Annual International Conference of the IEEE*. IEEE, 2015, pp. 6679–6683.
- [36] S. W. Lee, J. Verghese, R. Holtzer, J. R. Mahoney, and M. Oh-Park, “Trunk sway during walking among older adults: Norms and correlation with gait velocity,” *Gait & posture*, vol. 40, no. 4, pp. 676–681, 2014.
- [37] S. J. Ali, A. N. Ansari, A. Rahman, S. Imtiyaz, and B. Rashid, “Post-stroke hemiplegic gait: A review,” *The Pharma Innovation*, vol. 3, no. 8, Part A, 2016.
- [38] J. Rodda and H. Graham, “Classification of gait patterns in spastic hemiplegia and spastic diplegia: a basis for a management algorithm,” *European Journal of Neurology*, vol. 8, no. s5, pp. 98–108, 2001.
- [39] M. E. Morris, C. L. Martin, and M. L. Schenkman, “Striding out with parkinson disease: evidence-based physical therapy for gait disorders,” *Physical Therapy*, vol. 90, no. 2, p. 280, 2010.
- [40] Y. P. Huang, S. M. Bruijn, J. H. Lin, O. G. Meijer, W. H. Wu, H. Abbasi-Bafghi, X. C. Lin, and J. H. van Dieën, “Gait adaptations in low back pain patients with lumbar disc herniation: trunk coordination and arm swing,” *European Spine Journal*, vol. 20, no. 3, pp. 491–499, 2011.
- [41] S. Choi, I.-H. Youn, R. LeMay, S. Burns, and J.-H. Youn, “Biometric gait recognition based on wireless acceleration sensor using k-nearest neighbor classification,” in *Computing, Networking and Communications (ICNC), 2014 International Conference on*. IEEE, 2014, pp. 1091–1095.

- [42] N. Shibuya, B. T. Nukala, A. Rodriguez, J. Tsay, T. Nguyen, S. Zupancic, and D. Y. Lie, “A real-time fall detection system using a wearable gait analysis sensor and a support vector machine (svm) classifier,” in *Mobile Computing and Ubiquitous Networking (ICMU), 2015 Eighth International Conference on*. IEEE, 2015, pp. 66–67.
- [43] S. Hochreiter and J. Schmidhuber, “Long short-term memory,” *Neural computation*, vol. 9, no. 8, pp. 1735–1780, 1997.
- [44] I. Goodfellow, Y. Bengio, and A. Courville, *Deep learning*. MIT press, 2016.
- [45] A. Ben-Hur and J. Weston, “A user’s guide to support vector machines,” *Data mining techniques for the life sciences*, pp. 223–239, 2010.
- [46] C.-C. Chang and C.-J. Lin, “Libsvm: a library for support vector machines,” *ACM Transactions on Intelligent Systems and Technology (TIST)*, vol. 2, no. 3, p. 27, 2011.
- [47] D. M. Powers, “Evaluation: from precision, recall and f-measure to roc, informedness, markedness and correlation,” 2011.
- [48] C.-W. Hsu, C.-C. Chang, C.-J. Lin *et al.*, “A practical guide to support vector classification,” 2003.
- [49] F. Pedregosa, G. Varoquaux, A. Gramfort, V. Michel, B. Thirion, O. Grisel, M. Blondel, P. Prettenhofer, R. Weiss, V. Dubourg, J. Vanderplas, A. Passos, D. Cournapeau, M. Brucher, M. Perrot, and E. Duchesnay, “Scikit-learn: Machine learning in Python,” *Journal of Machine Learning Research*, vol. 12, pp. 2825–2830, 2011.